AIAA Aviation Forum and ASCEND co-located Conference Proceedings
29 July - 2 August 2024, Las Vegas, Nevada
AIAA AVIATION FORUM AND ASCEND 2024
10.2514/6.2024-4391

Numerical Investigation of Leakage of High-amplitude Sound in Ill-fitting Earplugs

Haocheng Yu*, Krishan K. Ahuja†, Lakshmi N. Sankar‡, and Spencer H. Bryngelson§
Georgia Institute of Technology, Atlanta, GA 30332

We present a numerical investigation of high-pressure sound waves through small orifice openings, focusing on earplug leakage. Our long-term goal is to improve earplug design in loud environments. Our contribution to earplug leak mechanics builds upon prior art that identifies the conversion of high-amplitude sound when passing through small openings into vorticity as a dominant dissipation mechanism in resonant acoustic liners. This quantifies the rate of kinetic energy transfer to the shed vortices, which can exceed the acoustic viscous dissipation rate. This provides a detailed understanding of the energy dissipation mechanisms when high-pressure sound waves propagate through small leaks.

I. Nomenclature

E	=	Mixture total energy
K	=	Dimensionless term representing expansion and compression in mixture regions
N	=	Number of frequency bands in broadband wave prescription
$\mathbf{F}$	=	Flux tensor
$\mathbf{I}$	=	Identity matrix
$\mathbf{T}$	=	Viscous stress tensor
$\widehat{R}$	=	Complex pressure amplitude reflection coefficient
S_j	=	The spectral power level of the j^{th} frequency band
c	=	Speed of sound
d	=	Height of the 2D orifice opening
f_j	=	The center frequency of the j^{th} frequency band
$\mathbf{h}$	=	Non-conservative variables vector
$\mathbf{q}$	=	State variables vector
r	=	Bandwidth growth factor
$\mathbf{r}$	=	Unit vector
$\mathbf{s}$	=	Source vector
t	=	Time
$\mathbf{u}$	=	Velocity field vector
$\mathbf{u_1}$	=	Horizontal component of velocity
x	=	First component of the Cartesian coordinate system
y	=	Second component of the Cartesian coordinate system
z	=	Third component of the Cartesian coordinate system
TL	=	Transmission loss
Δf	=	The bandwidth of the SPL spectrum
Δf_j	=	The bandwidth of the j^{th} frequency band
α_1	=	Volume fraction of the first fluid
α_2	=	Volume fraction of the second fluid
χ_j	=	The random phase shift of the j^{th} frequency band

*Graduate Research Assistant, School of Computational Science and Engineering, Daniel Guggenheim School of Aerospace Engineering, AIAA Student Memeber
†Regents Professor, Daniel Guggenheim School of Aerospace Engineering; Regents Researcher and Chief, Aerospace and Acoustics Technologies, GTRI, AIAA Fellow.
‡Regents Professor, Daniel Guggenheim School of Aerospace Engineering; AIAA Fellow.
§Assistant Professor, School of Computational Science and Engineering, Daniel Guggenheim School of Aerospace Engineering.

δ = Stokes boundary layer thickness
δ_l = Sample thickness of the leaks in the 2D ear model
λ = Acoustic wavelength
$\boldsymbol{\omega}$ = Vorticity vector in 3D
ρ = Mixture density
ρ_1 = Species density of the first fluid
ρ_2 = Species density of the second fluid
τ_π = Absorption coefficient

II. Introduction

The study of acoustic liners and their dissipation mechanisms has been a topic of interest for many researchers due to their significant role in noise reduction in various applications, such as aircraft engines and ear protection devices [1–6]. A dominant dissipation mechanism identified in resonant acoustic liners is vortex shedding, which occurs at the mouths of the resonators when high-amplitude sound waves propagate through them [1, 4, 7].

Sound passage through leakage paths in an ill-fitting earplug is similar to a passage through a small orifice with varying length and cross-section. The propagation of sound waves through small orifice openings has been studied to understand the dissipation of high Sound Pressure Level (SPL) acoustic energy [8, 9]. Several studies have also demonstrated the presence of air leaks in ill-fitting earplugs, which can compromise their effectiveness in noise attenuation [10–14]. It has been found that the presence of leakages and the insertion depth of earplugs are mainly responsible for the variability of the predicted earplug's so-called insertion loss at frequencies less than 1 kHz [9]. Another factor that influences the performance of earplugs is the occlusion effect, which corresponds to increased auditory perception when the ear canal is blocked. This effect, along with the insertion loss, is a useful measure of earplug performance [8].

Studies have investigated the behavior of flow through orifices, showing that when pressurized turbulent flow or laminar fluid flow passes through an orifice, it creates sound waves, disturbances, and pressure fluctuations leading to flow acoustic interaction [15]. Previous simulations have provided valuable insights into the acoustic wave scattering and fluid perturbations inside confined orifice flow [16]. The interaction between acoustic feedback and vortex shedding in combination with acoustic liners has been another area of interest [17]. This interaction is particularly relevant when considering the leakage in earplugs, which can be analogous to the resonator openings in acoustic liners.

Given extensive numerical simulations and experimental works to investigate the characteristics of acoustic liners and the propagation of sound waves through small orifice openings, we still have gaps in our understanding of the dissipation mechanisms when high-amplitude sound waves propagate through small air leaks because the shape of the air leaks varies and is irregular. Previous works on modeling and testing the air leaks in ill-fitting earplugs have attempted to model these small leaks as small orifice openings and experimentally measured the effects of the leaks in loud environments [18].

We work to extend this body of research by simulating the propagation of high-amplitude discrete tones through small air leaks in modeled ear canals with ill-fitting earplugs. We focus on quantifying the energy dissipated by vortices based on the absorption coefficient, a quantity of interest for noise reduction. Simulations based on the Navier-Stokes equations represent the conversion mechanism between loud sound and generated vortices. The results of this investigation enable the design and optimization of earplugs and similar devices, with potential implications for improving noise reduction in loud environments such as fighter jet carriers.

III. Numerical Methods

A. Compressible Multi-component Flow Solver

The numerical method employed in this study uses the open-source code MFC [19]. MFC solves governing partial differential equations for compressible multi-fluid multi-phase flows. The five-equation model of Kapila et al. [20] follows in (1) and (2) and is used as the governing equations of the system for this study. It consists of advection conservation, mass conservation for each fluid, momentum and energy conservation for the mixture, a stiffened-gas equation of state, and an additional set of equations for the volume fractions of the fluids. This model can capture the complex interactions between liquid or gas fluids, including the propagation of sound waves through small orifice

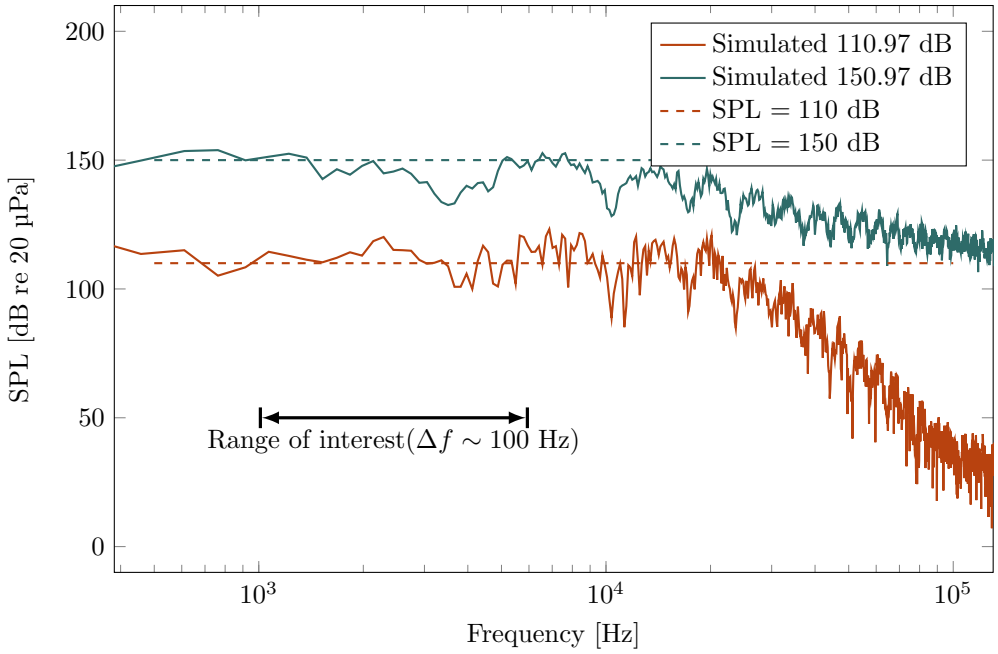

Fig. 1 Acoustic power spectrum of the simulated broadband sound following the formulation of Tam et al. [22].

openings. The governing equations we use are

$$\frac{\partial \mathbf{q}}{\partial t} + \nabla \cdot \mathbf{F}(\mathbf{q}) = \mathbf{s}(\mathbf{q}) \tag{1}$$

where $\mathbf{q}$ is the state variable vector, $\mathbf{F}$ is the flux tensor, and $\mathbf{s}$ are the source terms. The representation of the variables of the PDE is

$$\mathbf{q} = \begin{bmatrix} \alpha_1 \\ \alpha_1\rho_1 \\ \alpha_2\rho_2 \\ \rho\mathbf{u} \\ \rho E \end{bmatrix}, \quad \mathbf{F} = \begin{bmatrix} \alpha_1\mathbf{u} \\ \alpha_1\rho_1\mathbf{u} \\ \alpha_2\rho_2\mathbf{u} \\ \rho\mathbf{u}\mathbf{u} + p\mathbf{I} - \mathbf{T} \\ (\rho E + p)\mathbf{u} - \mathbf{T}\cdot\mathbf{u} \end{bmatrix}, \quad \mathbf{s} = \begin{bmatrix} 0 \\ f_g f_\delta / a \\ f_g f_\delta / a \\ f_g f_\delta \mathbf{r} \\ 0 \end{bmatrix} \tag{2}$$

where ρ, $\mathbf{u}$, and p are the mixture density, velocity, and pressure, respectively. α_k is the volume fraction of the component k, $\mathbf{T}$ is the viscous stress tensor with negligible bulk stresses, and $\mathbf{I}$ is the identity matrix. E is the total energy of the mixture. The nonconservative source terms in $\mathbf{s}$ corresponding to the one-way plane wave source of Maeda and Colonius [21], where f_g is the time-dependent amplitude for monopole and dipole sources, f_δ is the Gaussian monopole support function, a is the mixture speed of sound, and $\mathbf{r}$ is the unit vector. For this study, all sound waves are assumed to be harmonic, meaning that the time-dependent amplitude f_g is sinusoidal with time.

The spatial discretization of the governing equations is achieved using a finite volume method. The finite-volume method is particularly suitable for problems involving complex geometries and flows, such as propagating high-amplitude sound through small orifice openings. The temporal discretization is performed using a TVD Runge-Kutta method with third-order accuracy. This explicit time-stepping scheme provides high accuracy and stability for many problems, including the propagation of high-amplitude sound waves. In addition, the high-order Weighted Essentially Non-Oscillatory (WENO) scheme [23] is used to reconstruct the solution to capture sharp gradients in the high-amplitude solution without introducing spurious oscillations.

In addition to discrete tones, we also used a broadband acoustic source based on Tam et al. [22] to study the energy dissipation of different acoustic sources for the effects of leaks. The prescribed amplitude of the time-domain signal given in (3) is

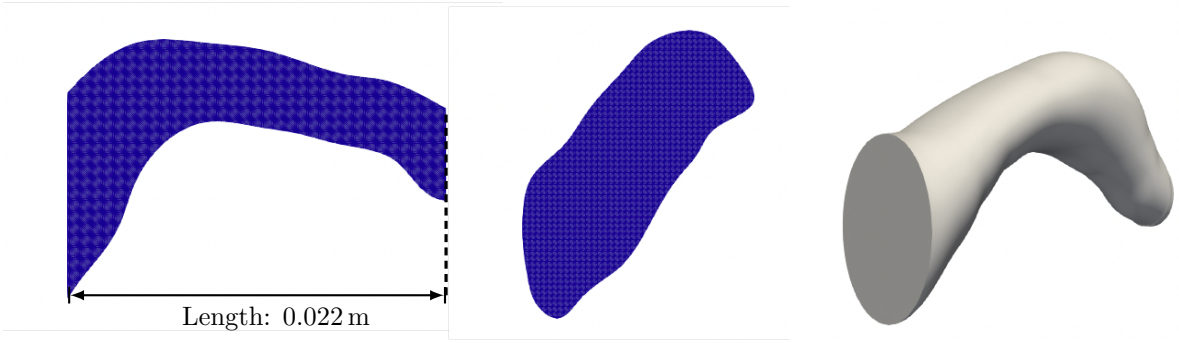

(a) 2D Ear canal **(b) 2D Ear plug** **(c) 3D canal**

Fig. 2 2D Models of the (a) ear canal and (b) ear plug, and (c) 3D model of the ear canal.

$$f_g(t) = \sum_{j=1}^{N} \sqrt{2\Delta f_j S_j} \cos(f_j t + \chi_j) \tag{3}$$

where $f_g(t)$ is the pressure amplitude as a function of time, N is the number of frequency bands in the prescribed spectrum, Δf_j is the width of the j^{th} band of the prescribed spectrum, S_j is the spectrum level at the j^{th} band, f_j is the center frequency of the j^{th} band and χ_j is a random phase shift between 0 to π for the j^{th} band. The prescribed bandwidth follows eq. (4) which are

$$\Delta f_j = r\,\Delta f_{j-1} \quad \text{and} \quad \Delta f_1 = 5000\left(\frac{r-1}{r^N - 1}\right), \tag{4}$$

where $r = 1.01$ and $N = 100$.

MFC is a GPU-accelerated and scalable codebase, so we can conduct sufficiently large simulations in short wall-times [24–26], even for broadband acoustic noise. The simulated power spectrum is shown in fig. 1. The spectral level at the frequency range of interest (1 kHz to 6 kHz) is close to the prescribed value. This shows the feasibility of using this method to simulate broadband acoustic wave with constant average SPL in the frequency range of interest.

B. Model Parameter Design

We used a ray-tracing algorithm to convert ASCII STL files, such as modeled orifices, earplugs, and ear canals, into structured computational grids for applying the numerical methods in section III.A. The ear canal models are 2D (shown in fig. 2a) and 3D (fig. 2c) and follow from Stinson and Lawton [27].

We use uniformly structured meshes with equal cell sides. Previous work has found the acoustic-driven flow bounded by small silt resonators as small as 1 cm is laminar at a high incident level about 155 dB [28]. It is intuitive that the flow bounded by small air leaks is also laminar, even though vortical disturbance and its interaction with high-amplitude sound can lead to the transition to turbulence outside of leaks. The laminar condition with an oscillatory wave gives rise to a viscous Stokes layer inside small air leaks [22]. We performed a grid convergence study and found that the fifth-order WENO scheme requires at least 20 cells to resolve the wavelength of the viscous Stokes layer. This study uses 10^4 cells per wavelength for 2D simulation and 500 cells per wavelength for 3D simulation to ensure negligible dissipation due to numerical errors.

C. Method Validation

To substantiate the reliability of our numerical methods, we create a 2D simulation featuring a 150 dB discrete tone as a plane wave propagating through an orifice. The opening of this orifice is meticulously scaled to be $1/28$ of the domain height to repeat the simulations performed in Tam et al. [1]. We use reflective boundary conditions in the horizontal direction, and the vertical boundaries are impermeable slip walls. This simulation framework was instrumental in visualizing the formation of a vortex street around the orifice openings. The resultant vortex patterns

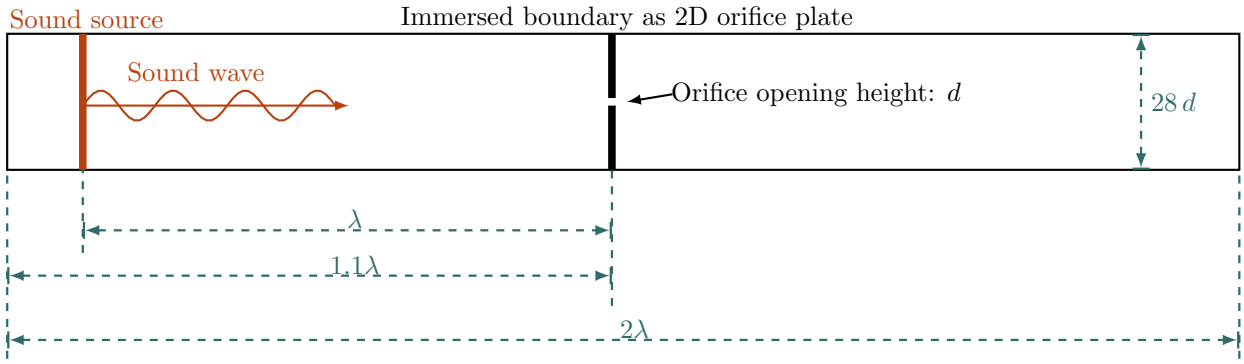

(a) Schematic of the computational domain with acoustic source (not to scale) where $28d \ll \lambda$.

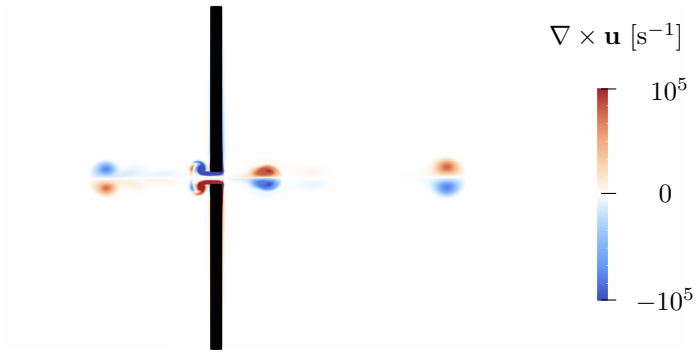

(b) Visualization of the vorticity.

Fig. 3 Visualization of flow through the orifice slit. (a) Schematic and (b) vorticity $\nabla \times \mathbf{u}$.

advecting both upstream and downstream, indicative of the generation of jet flow at the orifice mouth, are illustrated in fig. 3. This visual evidence supports our methodological approach to understanding wave propagation and vortex generation in loud environments.

The following discussion only holds for plane-wave, normal-incidence acoustic sources, such as the one described below. Here, the sound power absorption coefficient is referred to as the absorption coefficient,

$$\tau_\pi = 1 - |\widehat{R}|^2, \tag{5}$$

where $\widehat{R}$ is the complex pressure reflection coefficient that represents the ratio of the complex pressure amplitude of the reflected wave to that of the incident one. Here, $|\widehat{R}|^2$ represents the percentage of sound power that is reflected from an acoustic barrier. Thus, the absorption coefficient measures the reduction in sound as it passes through an acoustic barrier or the percentage of the sound power dissipated through the barrier, which could be an orifice silt, a leak, or a wall. Here, we compute the absorption coefficient for different frequencies.

In the 2D simulation described in fig. 3, we recorded pressure at two points along the horizontal center-line of the domain. These points are 3 cm and 2 cm upstream from the orifice opening. Pressure measurements were taken at each time step (0.1 µs increments). The sampling frequency of the recorded time history is as large as the inverse of the simulation time step. The recorded pressure time history computes the complex pressure reflection and absorption coefficients. Following Tam et al. [22] and Borges Mendes and De Araújo Nunes [30], we calculate the absorption coefficient based on the recorded time history. Figure 4 shows and compares the absorption coefficient spectra to previous work. Our analysis indicates that our method aligns well with previously established results, demonstrating its accuracy in simulating orifice openings in loud environments.

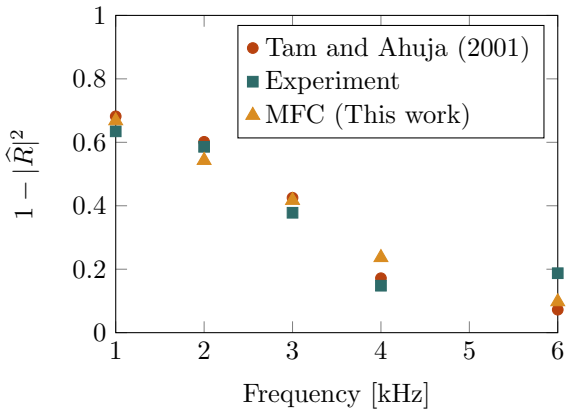

Fig. 4 Comparison of absorption coefficient spectra among numerical data and experiment of Ahuja et al. [29].

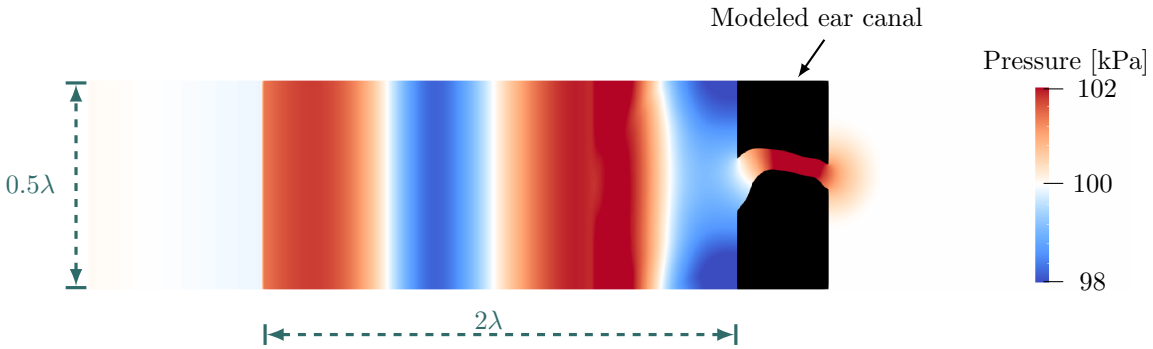

Fig. 5 Pressure distribution in 2D modeled ear canal with 150.97 dB **(pressure amplitude** 1 kPa**) and** 5 kHz **discrete tone. The distribution with lower amplitude discrete tones is similar to that shown in this figure.**

IV. Numerical Results

We simulate the 2D-modeled ear canal without using earplugs for various SPL environments. Figure 5 shows the particle velocity distribution within the ear canal. This step ensures an accurate translation of the STL files onto the computational grid. The pressure distribution and waveform in the 2D modeled ear canal offer insight into the behavior of sound waves within this complex anatomical structure.

We simulate the 2D ear canal with a modeled ill-fitting earplug and observe the effects when the sound amplitude varies. Figure 7 shows the translated 2D ear canal model with an ill-fitting earplug. We use the same method described in section III.C to compute the absorption coefficient based on the amplitude time history at the numerical probes.

Figure 8 compares the absorption coefficient in different acoustic environments. The simulated absorption coefficient in a loud environment is higher than in a quieter one. This result is expected, as we measured higher absorption at the orifice opening in louder environments. However, we did not observe vortices inside leaks. Since there is no published relevant empirical study, we don't have a specific answer to this phenomenon. We hypothesize that the thickness of the Stokes boundary layer can be comparable to the size of the leaks due to the excessively narrow gaps between the earplug and ear model. The Stokes boundary layer is given by Van Overveld et al. [31] as $\delta \sim \sqrt{\nu\lambda/c}$, where ν is the kinematic viscosity, λ is the acoustic wavelength, and c is the speed of sound.

As mentioned in section III.B, we use 10^4 cells per wavelength in the 2D simulations. The approximated thickness of the leaks in our 2D simulation based on fig. 7b is $\delta_l \sim \lambda/500$, and the ratio of the Stokes boundary thickness to the leak thickness is

$$\frac{\delta}{\delta_l} \sim \frac{1}{10\sqrt{\lambda}} \tag{6}$$

with the assumption that the medium air is at normal temperature and pressure. The thickness ratio is close to one

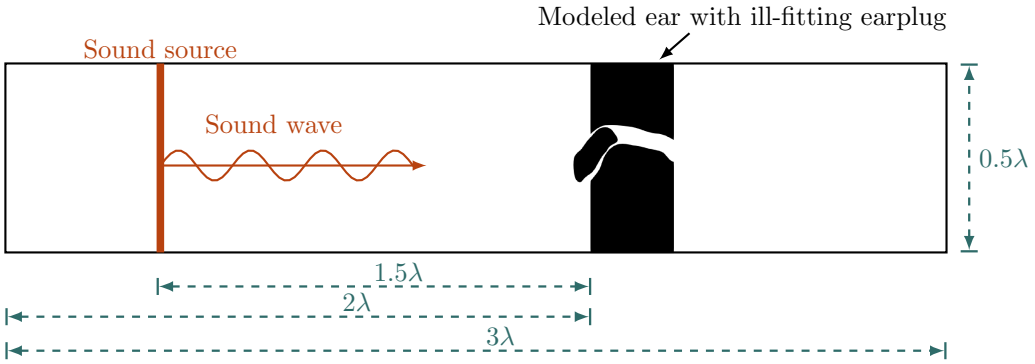

Fig. 6 Schematic of the computation domain with a 2D modeled ear and earplug.

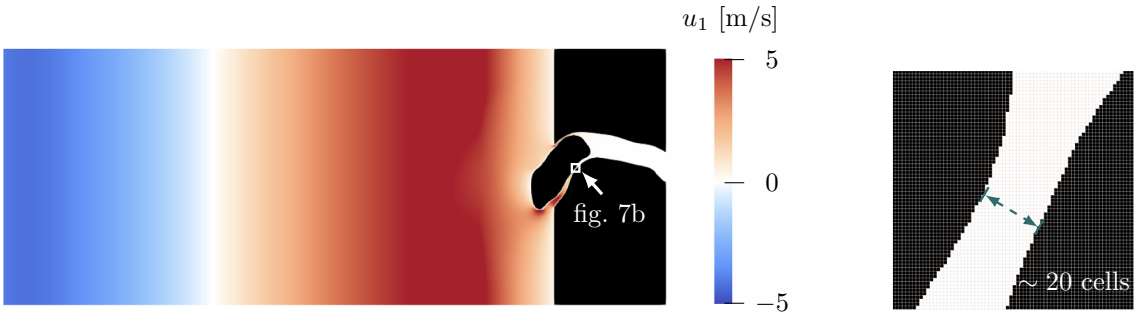

(a) Horizontal-component velocity color map. **(b) Magnified grid of the leak.**

Fig. 7 Simulation visualization of the 2D modeled ear canal with an ill-fitting earplug. (a) Horizontal velocity u_1 and (b) magnified grid of leak region of (a).

when $\lambda \leq 0.01$. Considering that the Stokes boundary layer exists on both the upper and lower edges of the leaks and that the thickness of the simulated leak is smaller than the orifice opening, the flow inside the leaks cannot reach the maximum speed at which it can move in unbounded conditions. The particle velocity at the entrance and exit of the gaps is insufficient to form significant vortices. Future research will focus on understanding the dynamics of the Stokes boundary layer on a curved surface and the vortex generation mechanism.

The 2D simulation of the modeled ear canal with ill-fitting earplugs shows that the absorption coefficient of the ill-fitting earplug is higher in louder environments ($\geq$ 149 dB) compared to quieter environments ($\leq$ 120 dB). This finding suggests that the vortex's dissipation mechanism's effectiveness can be enhanced in loud environments with air leaks.

We extended the work to 3D simulations using the same computational method as the 2D simulations. Figure 9a shows the section view of the translated 3D ear canal model with an ill-fitting earplug model. The model shown is symmetrical about the x–y plane denoted in fig. 9a. Therefore, the removed half is symmetrical to the half shown in the figure. In the visualization below, we can observe the internal vorticity by cutting the model in half. The plane wave assumption still holds in 3D simulations. The acoustic source plane is placed $\frac{3\lambda}{2}$ away from the inlet of the modeled ear canal, and the direction of the wave is perpendicular to the $y-z$ plane. We continue to the symmetrical reflective termination for the positive x domain boundary while the negative x domain boundary is a non-reflective subsonic buffer boundary based on Thompson [32]. An impermeable slip boundary condition is used for the domain boundaries in the y and z directions.

We plot a vorticity color map to determine the presence of vorticity near the exit of the ear canal model in fig. 9b. We observe that the upper edge of the ear canal model, which is relatively sharp, exhibits a more significant vorticity magnitude compared to the lower, smoother edge in the ear canal. This difference in vorticity suggests that the sharp edge may contribute to enhanced energy absorption. Like the 2D simulation, fig. 10 compares the absorption coefficient in different acoustic environments and source types. Higher absorption in a louder environment is observed, which

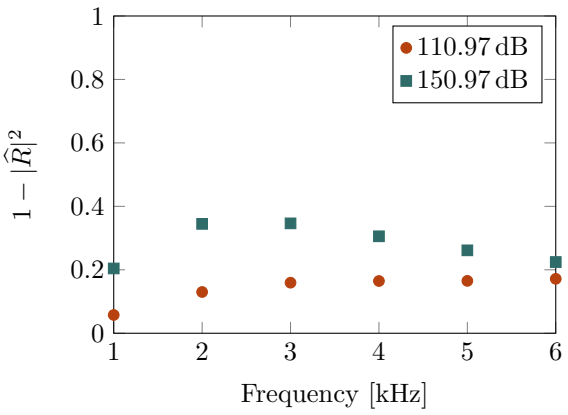

Fig. 8 Comparison of the absorption coefficient spectra of the modeled 2D ear canal with an ill-fitting earplug in a quieter and louder environment.

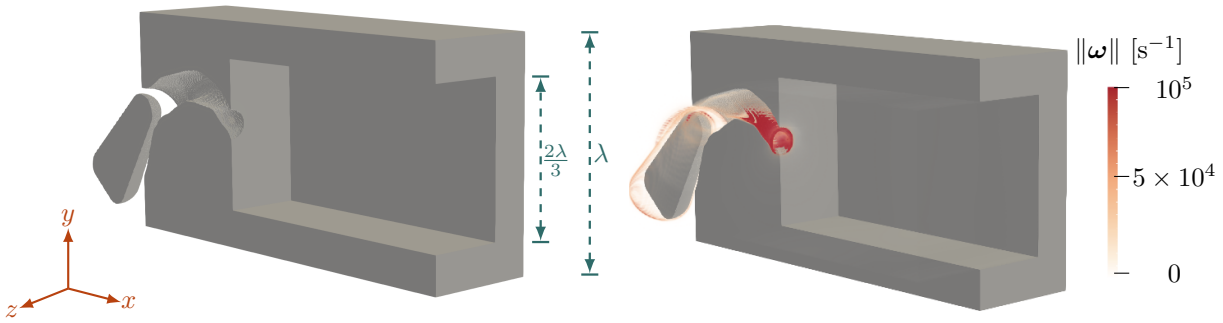

(a) Section view of the 3D model ear with earplug. **(b) Vorticity in the domain.**

Fig. 9 Simulation visualization of the 3D modeled ear canal with an ill-fitting earplug of (a) model schematics and (b) vorticity magnitude $\|\omega\|$.

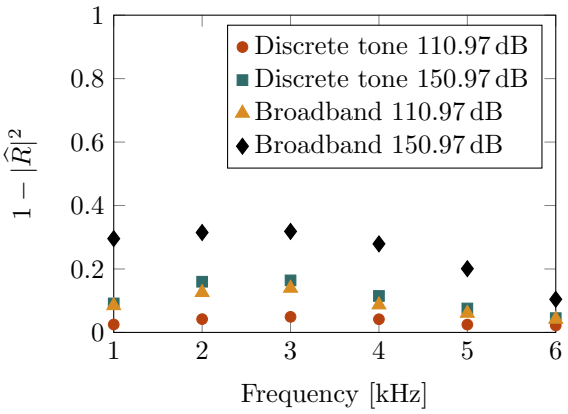

Fig. 10 Comparison of the absorption coefficient spectra of the modeled 3D ear canal with an ill-fitting earplug in a quieter and louder environment.

matches our expectations. We observed higher absorption with broadband acoustic wave, which is also expected as we observed higher vorticity magnitude using broadband wave than discrete tones even at an amplitude as low as 110.97 dB. Since the prescribed broadband wave has much higher overall SPL compared to the discrete tones, the broadband wave contains more energy so the absorption coefficient in the broadband environment is higher.

V. Concluding Remarks

In this study, we conducted 2- and 3-D simulations of the ear canal model to investigate the acoustic behavior of ill-fitting earplugs in various environments. Our simulations revealed several findings regarding the conversion of sound into vorticity and absorption coefficients.

We replicated the simulation of the loud sound wave passing through a small orifice opening using a high-order WENO scheme and compared it with previous works. The result agrees well. The comparison corroborates our methodology for examining wave propagation in loud environments where vortices are generated by consuming acoustic energy.

In scenarios involving an ill-fitting earplug, we observed variations in the absorption coefficient with changes in sound amplitude. The absorption coefficient is higher in louder environments. This result aligns with our expectations, as higher absorption is typically measured at the orifice opening under higher sound pressure levels.

No vortices were visualized inside the leaks, leading us to hypothesize that the particle velocity is inadequate to generate vortices because the thickness of the Stokes boundary layer is smaller than the gap between the earplug and the ear model. This hypothesis is supported by the formula provided by the calculated ratio of the Stokes boundary layer thickness to the leak thickness. Future works can focus on studying the dynamics of the laminar Stokes layer on a curved surface and the vortex generation mechanism where the thickness of the Stokes boundary layer is comparable to that of the leaks.

Acknowledgments

This work was based on the work (Yu et al. [18]) funded in part by the Georgia Institute of Technology Small Bets Internal Research and Development (IRAD) Program. This work used Bridges2 at the Pittsburgh Supercomputing Center and NCSA Delta through allocation TG-PHY210084 (PI Spencer Bryngelson) from the Advanced Cyberinfrastructure Coordination Ecosystem: Services & Support (ACCESS) program, which is supported by National Science Foundation grants #2138259, #2138286, #2138307, #2137603, and #2138296. SHB also acknowledges the resources of the Oak Ridge Leadership Computing Facility at the Oak Ridge National Laboratory, which is supported by the Office of Science of the U.S. Department of Energy under Contract No. DE-AC05-00OR22725. HY thanks Henry Le Berre for his guidance on the use of MFC and its features.

References

[1] Tam, C. K., Kurbatskii, K. A., Ahuja, K., and Gaeta Jr, R., "A numerical and experimental investigation of the dissipation mechanisms of resonant acoustic liners," *Journal of Sound and Vibration*, Vol. 245, No. 3, 2001, pp. 545–557.

[2] Jones, M. G., Watson, W. R., Nark, D. M., Howerton, B. M., and Brown, M. C., "A review of acoustic liner experimental characterization at NASA Langley," 2020.

[3] Yan, Q., Xue, D., Mu, Q., Yang, J., Gao, X., and Huang, W., "Acoustic Experimental Technology for Aircraft Nacelle Liner," *Aerospace*, Vol. 10, No. 1, 2023, p. 56.

[4] Tam, C. K., Pastouchenko, N., Jones, M. G., and Watson, W. R., "Experimental validation of numerical simulation for an acoustic liner in grazing flow," *19th AIAA/CEAS Aeroacoustics Conference*, 2013, p. 2222.

[5] Zheng, M., Chen, C., and Li, X., "Experimental investigation of factors influencing acoustic liner drag using direct measurement," *Aerospace Science and Technology*, Vol. 130, 2022, p. 107903.

[6] Habibi, K., and Mongeau, L., "Prediction of sound absorption by a circular orifice termination in a turbulent pipe flow using the Lattice-Boltzmann method," *Applied Acoustics*, Vol. 87, 2015, pp. 153–161.

[7] Dai, X., Jing, X., and Sun, X., "Discrete vortex model of a Helmholtz resonator subjected to high-intensity sound and grazing flow," *The Journal of the Acoustical Society of America*, Vol. 132, No. 5, 2012, pp. 2988–2996.

[8] Carillo, K., Sgard, F., Dazel, O., and Doutres, O., "Passive earplug including Helmholtz resonators arranged in series to achieve broadband near zero occlusion effect at low frequencies," *The Journal of the Acoustical Society of America*, Vol. 154, No. 4, 2023, pp. 2099–2111.

[9] Viallet, G., Sgard, F., Laville, F., and Nelisse, H., "Investigation of the variability in earplugs sound attenuation measurements using a finite element model," *Applied Acoustics*, Vol. 89, 2015, pp. 333–344.

[10] Groon, K. A., Rasetshwane, D. M., Kopun, J. G., Gorga, M. P., and Neely, S. T., "Air-leak effects on ear-canal acoustic absorbance," *The Journal of Ear and Hearing*, Vol. 36, No. 1, 2015, p. 155.

[11] Henriksen, V., "Using impedance measurements to detect and quantify the effect of air leaks on the attenuation of earplugs," *The Journal of the Acoustical Society of America*, Vol. 124, No. 1, 2008, pp. 510–522.

[12] Chordekar, S., Adelman, C., Sohmer, H., and Kishon-Rabin, L., "Soft tissue conduction as a possible contributor to the limited attenuation provided by hearing protection devices," *The Journal of Noise & Health*, Vol. 18, No. 84, 2016, p. 274.

[13] Rice, C., and Coles, R., "Design factors and use of ear protection," *Occupational and Environmental Medicine*, Vol. 23, No. 3, 1966, pp. 194–203.

[14] Berger, E. H., "Tips for fitting hearing protectors," *The Journal of Sound and Vibration*, Vol. 6, 1988, pp. 22–25.

[15] Kadam, A. R., and Chaudhari, M. B., "Acoustic study and behavior of flow through orifices," *Procedia Manufacturing*, Vol. 20, 2018, pp. 154–159.

[16] Chen, W., Wang, P., and Liu, Y., "Numerical simulation on the acoustic wave scattering and fluid perturbations inside confined orifice flow," *International Journal of Aeroacoustics*, 2023, p. 1475472X231183155.

[17] Hong, Z., Fu, Y., Chen, L., and Yang, M., "Experimental investigation on vortex sound interaction in self-induced acoustic resonance," *Journal of Sound and Vibration*, Vol. 548, 2023, p. 117510.

[18] Yu, H., Filloon, J., Ramsey, D. N., Ahuja, K. K., and Sankar, L. N., "Modelling and testing sound leakage in ill-fitting earplugs," *AIAA SCITECH 2022 Forum*, 2022, p. 2562.

[19] Bryngelson, S. H., Schmidmayer, K., Coralic, V., Meng, J. C., Maeda, K., and Colonius, T., "MFC: An open-source high-order multi-component, multi-phase, and multi-scale compressible flow solver," *Computer Physics Communications*, Vol. 266, 2021, p. 107396.

[20] Kapila, A., Menikoff, R., Bdzil, J., Son, S., and Stewart, D. S., "Two-phase modeling of deflagration-to-detonation transition in granular materials: Reduced equations," *Physics of Fluids*, Vol. 13, No. 10, 2001, pp. 3002–3024.

[21] Maeda, K., and Colonius, T., "A source term approach for generation of one-way acoustic waves in the Euler and Navier–Stokes equations," *Wave Motion*, Vol. 75, 2017, pp. 36–49.

[22] Tam, C. K., Ju, H., Jones, M. G., Watson, W. R., and Parrott, T. L., "A computational and experimental study of resonators in three dimensions," *Journal of Sound and Vibration*, Vol. 329, No. 24, 2010, pp. 5164–5193.

[23] Coralic, V., and Colonius, T., "Finite-volume WENO scheme for viscous compressible multicomponent flows," *Journal of Computational Physics*, Vol. 274, 2014, pp. 95–121.

[24] Elwasif, W., Godoy, W., Hagerty, N., Harris, J. A., Hernandez, O., Joo, B., Kent, P., Lebrun-Grandie, D., Maccarthy, E., Melesse Vergara, V., et al., "Application experiences on a GPU-accelerated arm-based HPC testbed," *Proceedings of the HPC Asia 2023 Workshops*, 2023, pp. 35–49.

[25] Radhakrishnan, A., Le Berre, H., and Bryngelson, S. H., "Scalable GPU accelerated simulation of multiphase compressible flow," *The International Conference for High Performance Computing, Networking, Storage, and Analysis (SC)*, Dallas, TX, USA, 2022, pp. 1–3.

[26] Radhakrishnan, A., Le Berre, H., Wilfong, B., Spratt, J.-S., Rodriguez Jr., M., Colonius, T., and Bryngelson, S. H., "Method for portable, scalable, and performant GPU-accelerated simulation of multiphase compressible flow," *Computer Physics Communications*, Vol. 302, 2024, p. 109238.

[27] Stinson, M. R., and Lawton, B., "Specification of the geometry of the human ear canal for the prediction of sound-pressure level distribution," *The Journal of the Acoustical Society of America*, Vol. 85, No. 6, 1989, pp. 2492–2503.

[28] Tam, C. K., and Kurbatskii, K. A., "Microfluid dynamics and acoustics of resonant liners," *AIAA journal*, Vol. 38, No. 8, 2000, pp. 1331–1339.

[29] Ahuja, K., Gaeta Jr, R., and D'Agostino, M., "High amplitude acoustic behavior of a slit-orifice backed by a cavity," *Technical Report NASA/CR-2000-210635*, 2000.

[30] Borges Mendes, C. O., and De Araújo Nunes, M. A., "Numerical methodology to obtain the sound absorption of materials by inserting the acoustic impedance," *Archives of Acoustics*, 2021, pp. 649–656.

[31] Van Overveld, T. J., Breugem, W.-P., Clercx, H. J., and Duran-Matute, M., "Effect of the Stokes boundary layer on the dynamics of particle pairs in an oscillatory flow," *Physics of Fluids*, Vol. 34, No. 11, 2022.

[32] Thompson, K. W., "Time-dependent boundary conditions for hyperbolic systems, II," *Journal of computational physics*, Vol. 89, No. 2, 1990, pp. 439–461.